Supporting information

In-situ exsolved Co nanoparticles coupled on $LiCoO_2$ nanofibers to induce oxygen electrocatalysis for rechargeable Zn-air batteries

Liangqi Gui,[a] Yuzhou Liu,[a] Jing Zhang,[a] Beibei He,[a,b,*] Qing Wang,[c] and Ling Zhao.[a,b,*]

[a]Faculty of Materials Science and Chemistry, China University of Geosciences, Wuhan, 430074, China.

[b]Zhejiang Institute, China University of Geosciences (Wuhan), Hangzhou, 311305, China.

[c]Department of Materials Science and Engineering, Pennsylvania State University, University Park, Pennsylvania 16802, USA.

*Corresponding author. Email: babyfly@mail.ustc.edu.cn (Beibei He), zhaoling@cug.edu.cn (Ling Zhao)

Experimental Section

Materials synthesis

Synthesis of $LiCoO_2$ and $Co@LiCoO_2$ nanofibers: $LiCoO_2$ nanofibers (LCO-NFs) were synthesized via an electrospinning method. First, cobalt nitrate hexahydrate ($Co(NO_3)_2•6H_2O$) and lithium nitrate ($LiNO_3$) were introduced into N, N-dimethylformamide (DMF) solvent to obtain an uniform solution. Subsequently, polyvinypyrrolidone (PVP, Mw = 1,300,000) was added to such solution, followed by stirring constantly for 4 h. The mass radio of total metal salt: PVP: DMF was 1: 1: 8. Then, the as-prepared spinning solution was transferred into a plastic syringe, followed by electrospinning at an voltage of 18 kV, a distance between needle and rolling collector of 15 cm, and a feeding rate of 0.3 mL h^{-1}. The obtained precursor nanofibers were dried at 60 ℃ in a vacuum oven for 12 h. Then, the dried fresh nanofibers were heat-treated at 600 ℃ for 2 h in air to gain the LCO-NFs. Finally, the LCO-NFs were annealing at 350 ℃ for 2 h in 5 % H_2 - 95 % Ar to form in-situ exsoluted $Co@LiCoO_2$ nanofibers (Co@LCO-NFs).

Preparation of $LiCoO_2$ bulk: The $LiCoO_2$ bulk (LCO-bulk) was prepared via a traditional sol-gel approach. Typically, 0.02 mol $LiNO_3$ and 0.02 mol $Co(NO_3)_2•6H_2O$ were dissolved in the deionized water, followed by the introduction of chelating agents of 0.04 mol citric acid and 0.06 mol EDTA. $NH_3•H_2O$ was applied to tune the pH value (~7). The obtained solution was heated till self-combustion occurred. Finally, the solid precursor was sintered at 600 ℃ for 2 h in air to obtain LCO-bulk.

Materials characterization

Crystal structures of as-prepared LCO-bulk, LCO-NFs and Co@LCO-NFs samples were analyzed via X-ray diffraction (XRD, Bruker D8-Focus). Morphologies of these resultant catalysts were observed by field-emission scanning electron microscope (FESEM, Hitachi SU-8010) and high-

resolution transmission electron microscopy (HRTEM, Tecnai G2 F20 U-TWIN). Surface electronic structures of catalysts were carried out by X-ray photo-electron spectroscopy (XPS, Kratos Axis Ultra DLD) equipped with $Al_{K\alpha}$ excitation source. Typical XPS spectra were fitted based on XPSPEAK software. Surface oxygen vacancies of catalysts were further examined by electron paramagnetic resonance (EPR) at room temperature on a Bruker-A300 EPR spectrometer. Hydrogen temperature programmed reduction (H_2-TPR) was performed via the AutoChem II 2920 instrument (Micromeritics, USA) equipped with a thermal conductivity detector (TCD) under 5% H_2-95% Ar atmosphere with temperature ranging from 25 ℃ to 400 ℃ at a heating rate of 10 ℃ min^{-1}.

Density functional theory calculations

First-principle calculations were performed by density functional theory (DFT) based on the Vienna Ab-initio Simulation Package (VASP) package.[1] Generalized gradient approximation (GGA) with Perdew− Burke−Ernzerhof (PBE) functional[2] were adopted to address the electronic exchange and correlation effects. Uniform G-centered k-points meshes with a resolution of 2π*0.03 $Å^{-1}$ and Methfessel-Paxton electronic smearing were applied for geometric optimization. The simulations were conducted with a cutoff energy of 500 eV. These settings ensure convergence of the total energies to within 1 meV per atom. Structure relaxation proceeded until all forces on atoms were less than 1 meV $Å^{-1}$ and the total stress tensor was within 0.01 GPa of the target value. In view of the strong-correlation of d electrons in Co, a U−J parameter of 5 eV was adopted.[3] For the construction of Co@$LiCoO_2$ heterostructure, we first spliced put double-layer $LiCoO_2$ on Co system along (001) direction since both materials adopt hexagonal structures and their lattice constants were matched. For the $LiCoO_2$ and Co@$LiCoO_2$ systems, their (100) planes served as the reaction surfaces, since they could predominantly expose Co atoms in an octahedral environment, and the vacuum space was 12 Å.

According to hydrogen electrode (CHE) model, the adsorption free energy for reaction intermediates, including OH^*, O^* and OOH^*, was expressed by the following equation:

$$\Delta G_{ads} = \Delta E_{ads} + \Delta E_{ZPE} - T\Delta S$$

Where ΔE_{ads} was the adsorption energy change of adsorbates, E_{ZPE} was the zero energy calculated from the vibrational frequencies, ΔS was the entropy change, and T was the room temperature. Generally, in alkaline media, a widely accepted OER reaction mechanism could be expressed as 4-elecetron process:

Step1: $^* + OH^- \rightarrow OH^* + e^-$

Step2: $OH^* + OH^- \rightarrow O^* + H_2O + e^-$

Step3 : $O^* + OH^- \rightarrow OOH^* + e^-$

Step4 : $OOH^* + OH^- \rightarrow O_2 + ^* + H_2O + e^-$

where * presented an adsorption site on the catalyst, and OH^*, O^*, and OOH^* denoted the corresponding absorbed intermediates. In the case of ORR, its reaction mechanism was the opposite to OER.

Electrochemical measurement

Catalyst ink, consisting of 4 mg of activated carbon, 16 mg of as-obtained catalyst, 3.9 mL of anhydrous ethanol and 0.1 mL of 5 wt% Nafion solution (Sigma-Aldrich), was prepared by ultrasonication for 30 minutes. Subsequently, the polished glassy carbon electrode with a diameter of 3 mm was covered by 4 μL of the resultant catalyst ink. For assessing the activity and durability of LCO-bulk, LCO-NFs and Co@LCO-NFs electrocatalysts, cyclic voltammogrom (CV), electrochemical impedance spectroscopy (EIS), linear sweep voltammogram (LSV), rotating ring-disk

electrode (RRDE) and chronoamperometry were carried out in an electrochemical station (CHI760E) with a standard three-electrode system. Glossy carbon electrode with a catalyst loading of 0.2830 mg cm^{-2} (0.2264 mg_{cat} cm^{-2}) was studied as the working electrode. Graphite rod electrode was used as the counter electrode. Hg/HgO electrode served as the reference electrode. And, 0.1 M KOH solution was applied as the electrolyte. The measured potential with iR correction was revised to reversible hydrogen electrode (RHE) potential.

Zn-air batteries test

Home-made Zn-air batteries were assembled with a configuration of an anode (Zn sheet), an electrolyte (6 M KOH and 0.2 M $Zn(CH_3COO)_2$) and an air electrode (carbon paper with catalyst loading of 1 mg_{cat} cm^{-2}). A mixture of commercial Pt/C and IrO_2 with a mass ratio of 1:1 were also studied as a referenced air electrode. A nickel mesh was applied as the current collector. The discharge process curves were gotten via the electrochemical station (CHI760E) with a two-electrode system. Discharge-charge performance of the batteries were performed by a multichannel battery testing system (LAND CT2001A) at a current density of 10 mA cm^{-2} with 5 min discharge and 5 min charge. Specific capacities of batteries were derived from the galvanostatical discharge plots.

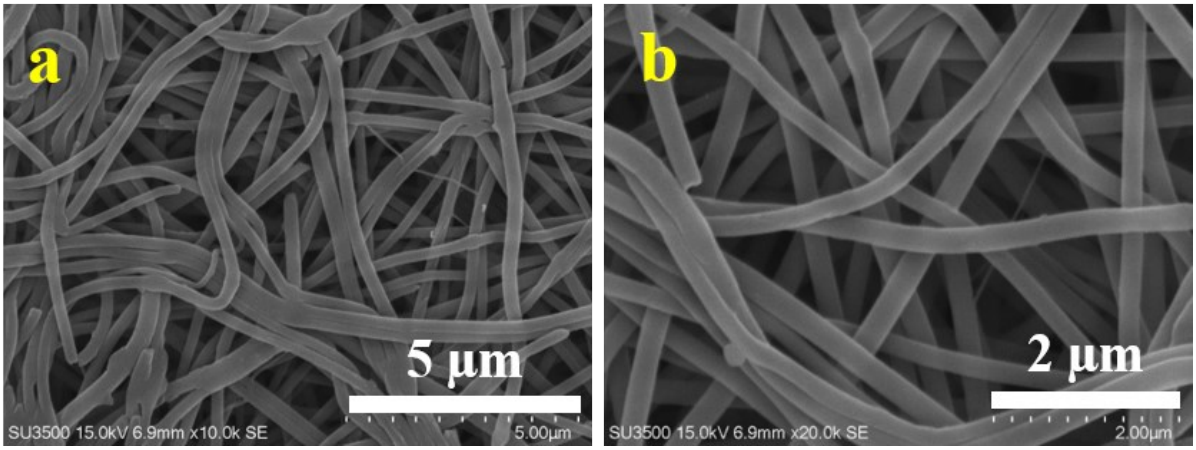

Figure S1. FESEM images of as-spun precursor nanofibers at different magnifications: (a)×10000, (b)×20000.

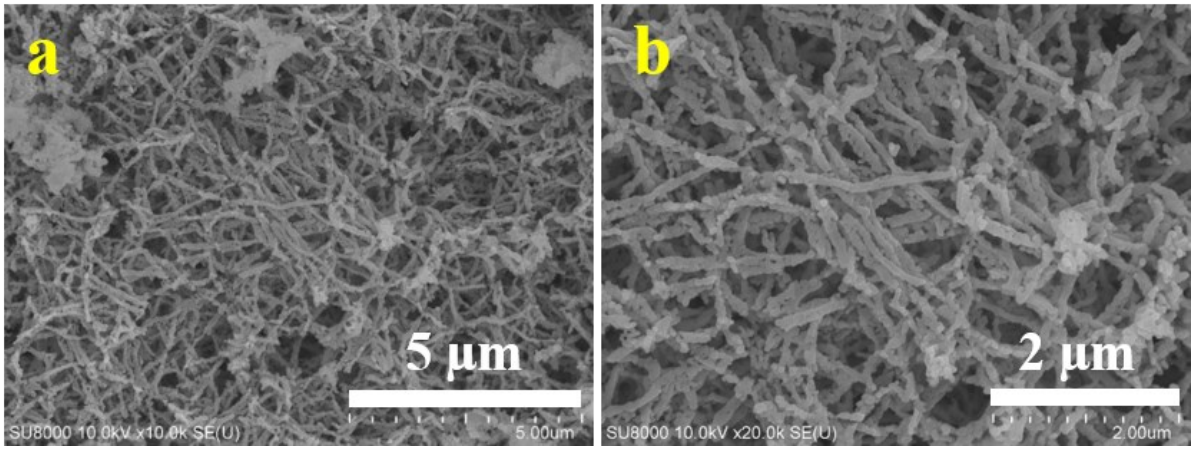

Figure S2. FESEM images of LCO-NFs at different magnifications: (a)×10000, (b)×20000.

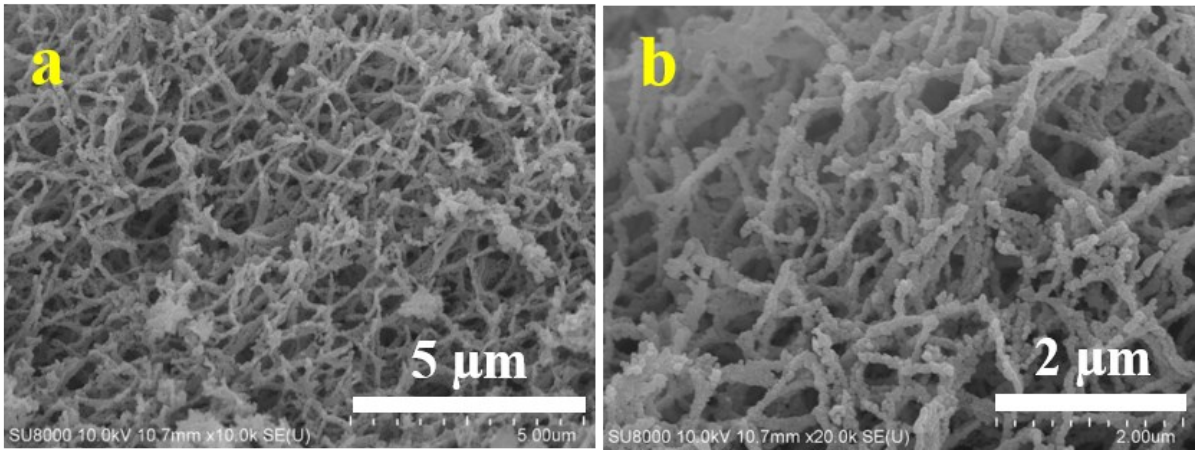

Figure S3. FESEM images of Co@LCO-NFs at different magnifications: (a)×10000, (b)×20000.

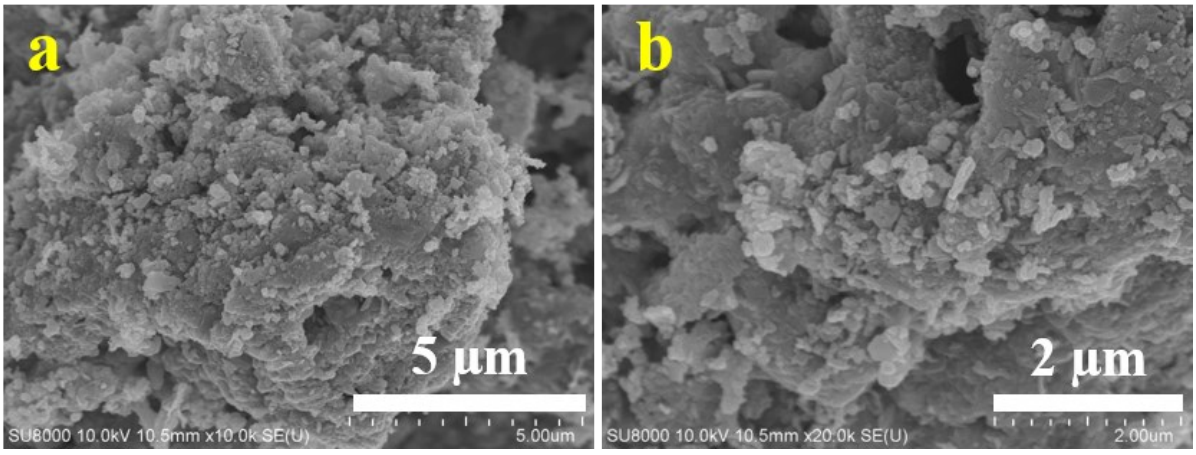

Figure S4. FESEM images of LCO-bulk at different magnifications: (a)×10000, (b)×20000.

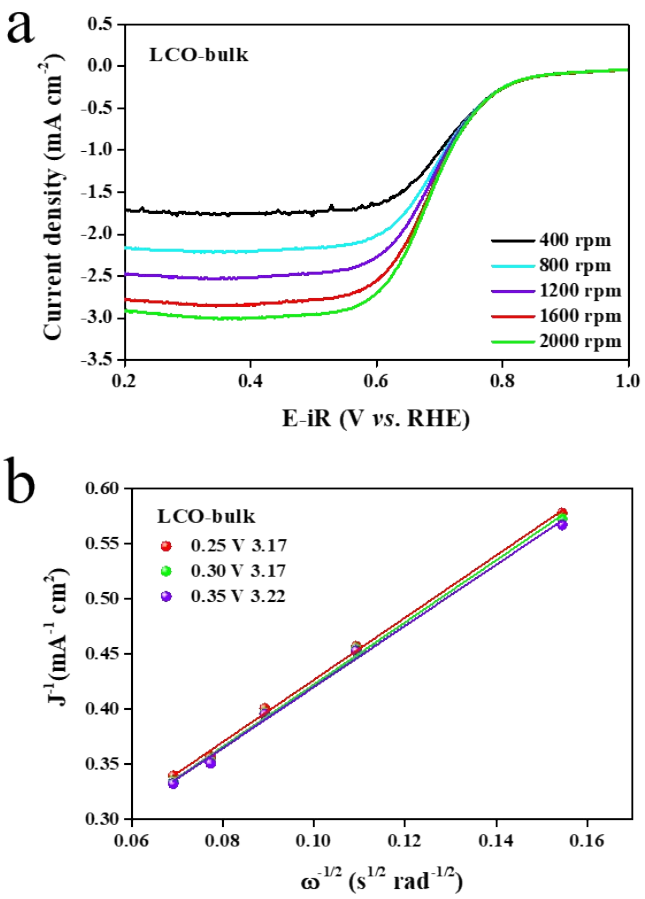

Figure S5. (a) Rotating-disk voltammograms of LCO-bulk catalyst with a sweep rate of 10 mV s^{-1} at the various rotation speeds rates in O_2-saturated 0.1 M KOH, (b) The corresponding Koutecky-Levich plots of LCO-bulk catalyst under different applied potentials.

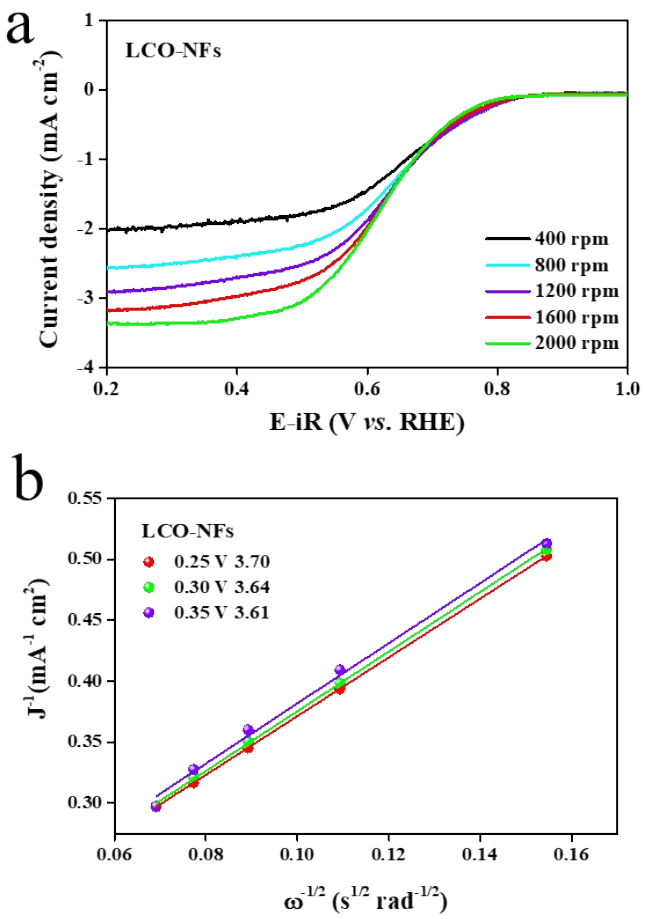

Figure S6. (a) Rotating-disk voltammograms of LCO-NFs catalyst with a sweep rate of 10 mV s^{-1} at the various rotation speeds rates in O_2-saturated 0.1 M KOH, (b) The corresponding Koutecky-Levich plots of LCO-NFs catalyst under different applied potentials.

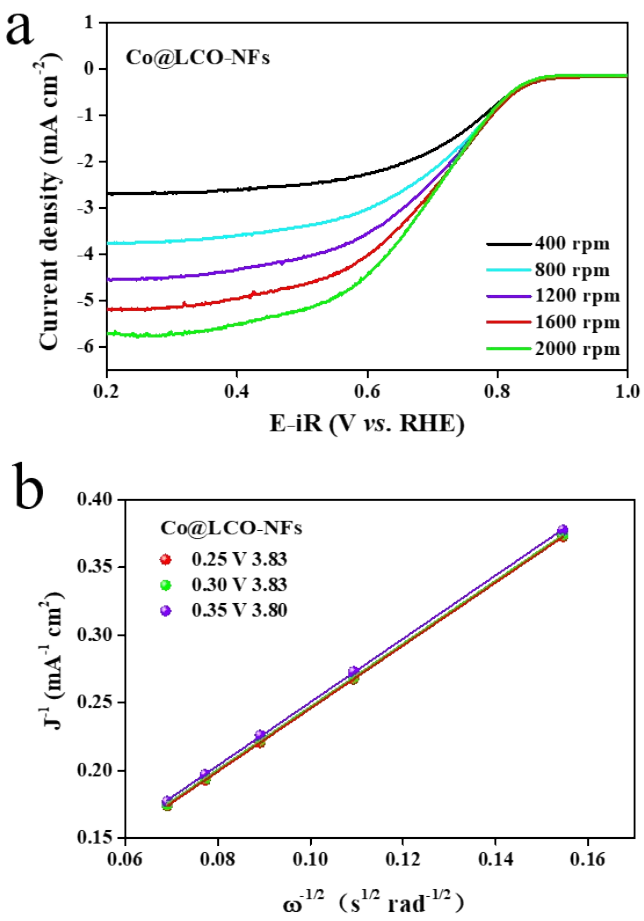

Figure S7. (a) Rotating-disk voltammograms of Co@LCO-NFs catalyst with a sweep rate of 10 mV s^{-1} at the various rotation speeds rates in O_2-saturated 0.1 M KOH, (b) The corresponding Koutecky-Levich plots of Co@LCO-NFs catalyst under different applied potentials.

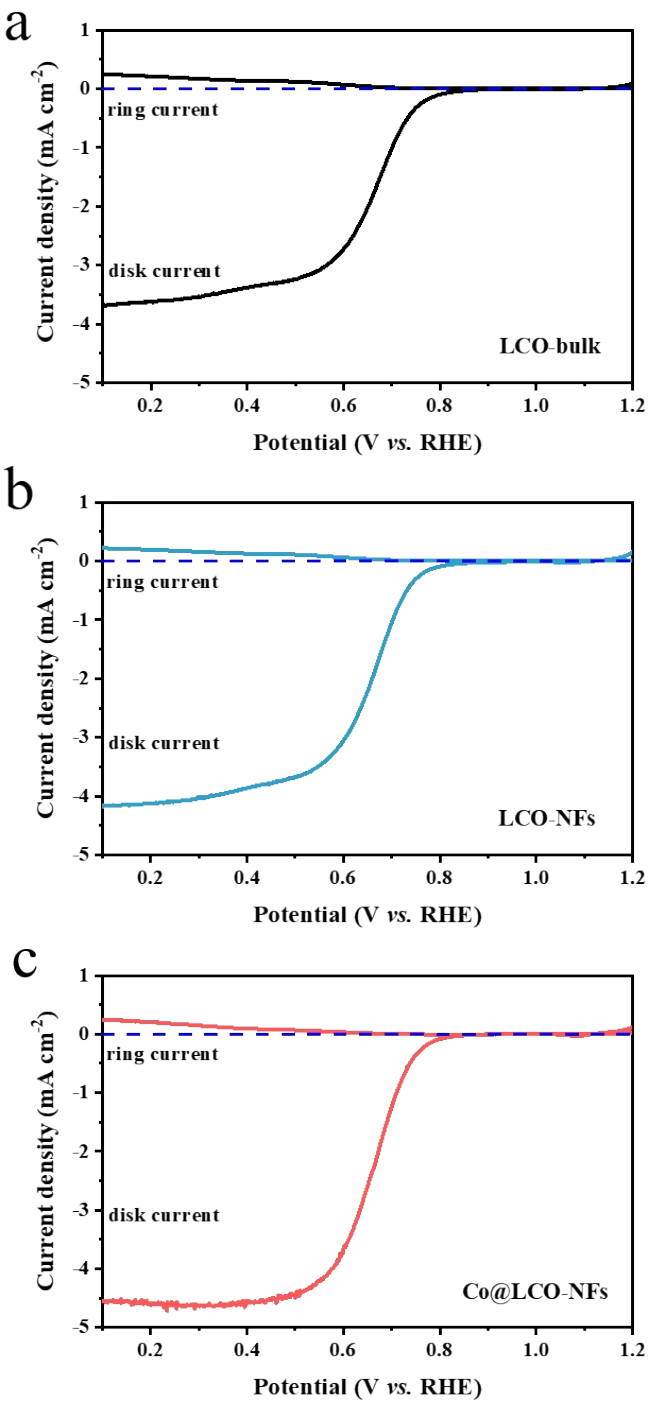

Figure S8. Rotating ring-disk electrode (RRDE) scans on (a) LCO-bulk, (b) LCO-NFs and (c) Co@LCO-NFs catalysts.

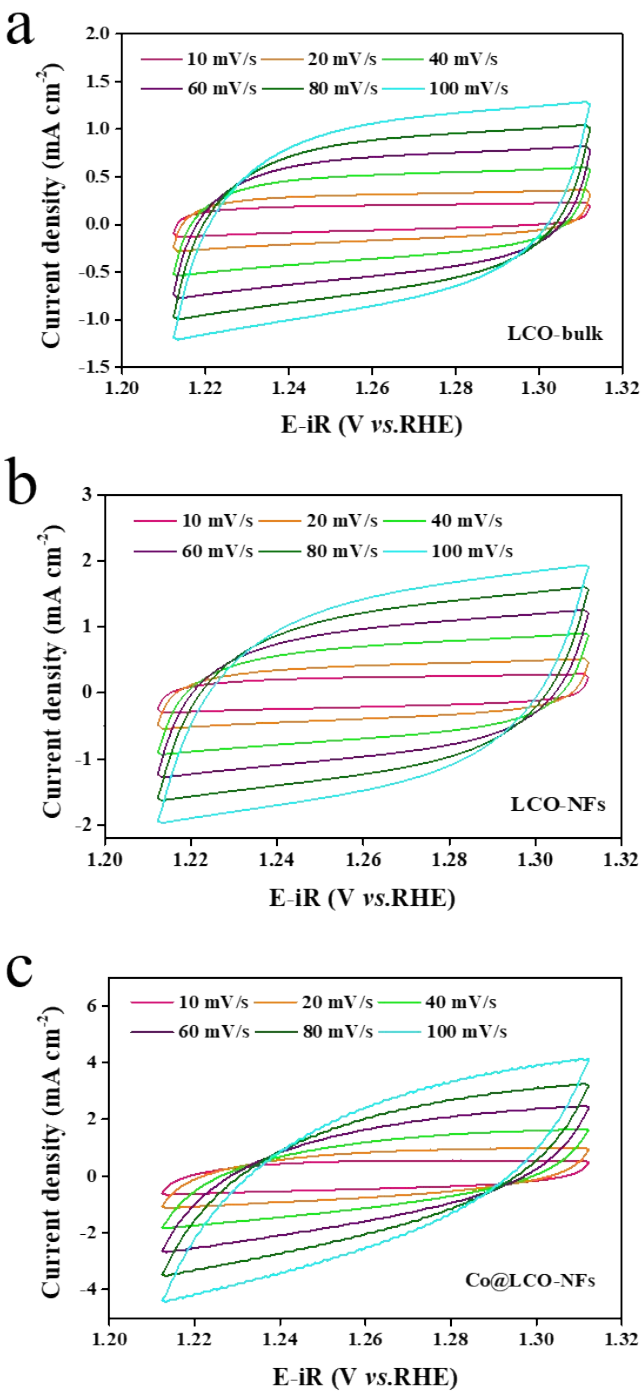

Figure S9. Electrochemical CV curves of (a) LCO-bulk, (b) LCO-NFs and (c) Co@LCO-NFs catalysts at different scan rates of 10, 20, 40, 60, 80, and 100 mV s^{-1}.

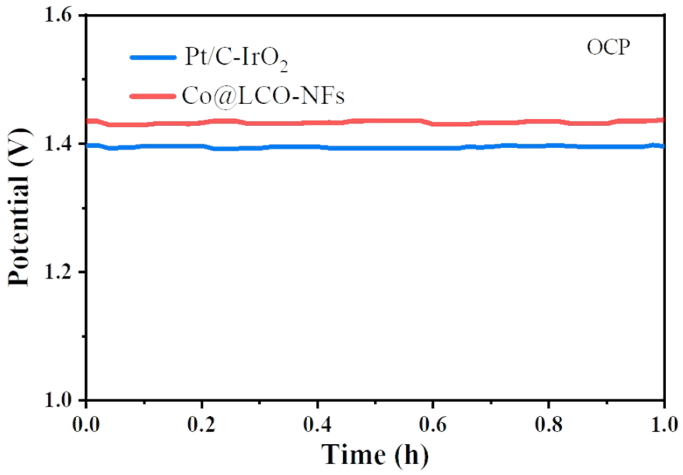

Figure S10. Open circuit voltage tests of Zn-air batteries with Co@LCO-NFs and Pt/C+IrO_2 air electrodes.

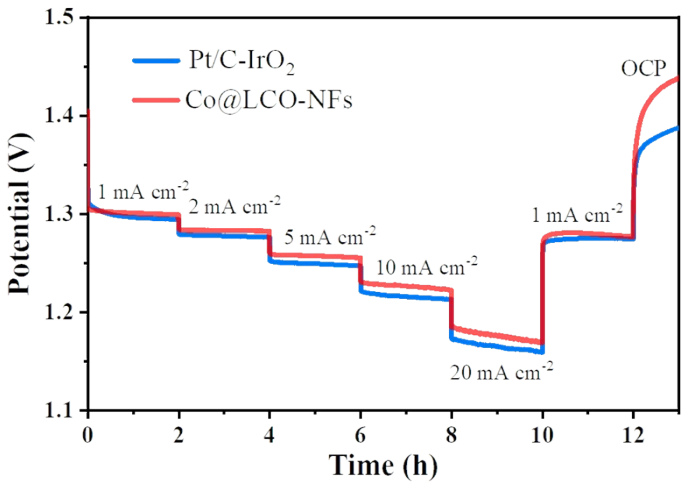

Figure S11. Voltage platforms at various discharge current densities of Zn-air batteries with Co@LCO-NFs and Pt/C+IrO_2 air electrodes.

Table S1. Co valence state concentration of LCO-NFs and Co@LCO-NFs catalysts derived from XPS peak deconvolution.

Electrocatalyst	Co^{2+}	Co^{3+}	Co^{0}
LCO-NFs	16.95 %	83.05 %	-
Co@LCO-NFs	30.33 %	51.64 %	18.03 %

Table S2. O 1s XPS peak deconvolution results of LCO-NFs and Co@LCO-NFs catalysts.

Electrocatalyst	O^{2-}	O_2^{2-}/O^-	OH^-/O_2	H_2O
LCO-NFs	41.99 %	19.95 %	17.24 %	20.82 %
Co@LCO-NFs	25.93 %	30.13 %	27.48 %	16.46 %

Table S3. Comparison of electrochemical performance of rechargeable Zn-air batteries with different electrodes.

Catalyst	Open circuit voltage (V)	Peak power density (mW cm^{-2})	Recharge ability	Specific capacity	Ref.
Co@LCO-NFs	**1.43**	**198**	**600 s / cycle for 1200 cycles**	**791 mAh g^{-1} at 10 mA cm^{-2}**	**This work**
Pt-Sr$(Co_{0.8}Fe_{0.2})_{0.95}P_{0.05}O_{3-\delta}$	1.40	122	1200 s / cycle for 240 cycles	790 mAh g^{-1} at 10 mA cm^{-2}	Adv. Energy Mater., 2019, 10, 1903271[4]
FePc@N,P-DC	1.45	120	200 s / cycle for 900 cycles	585 mAh g^{-1} at 10 mA cm^{-2}	Appl. Catal. B: Environ., 2020, 260. 118198[5]
$FeNi_3$@NC	1.39	139	3600 s / cycle for 30 cycles	756 mAh g^{-1} at 10 mA cm^{-2}	Appl. Catal. B: Environ., 2020, 268, 118729[6]
CuSA@HNCNx	1.51	202	600 s / cycle for 1500 cycles	793 mAh g^{-1} at 25 mA cm^{-2}	Appl. Catal. B: Environ., 2020, 268, 118746[7]
CoP-$PrBa_{0.5}Sr_{0.5}Co_{1.5}Fe_{0.5}O_{5+\delta}$ nanofibers	-	138	1200 s / cycle for 100 cycles	-	J. Mater. Chem. A., 2019, 7, 26607–26617[8]
Co-SAs@NC	1.46	105.3	-	897.1 mA h g^{-1} at 20 mA cm^{-2}	Angew. Chem., Int. Ed., 2019, 58, 5359-5364.[9]
Mn/Fe-HIB-MOF	~1.48	195	600 s / cycle for over 6000 cycles	769 mAh g^{-1} at 5 mA cm^{-2}	Energy Environ. Sci., 2019, 12, 727-738[10]
Cobalt-coordinated framework porphyrin with graphene	-	78	1200 s / cycle for 237 cycles	-	Adv. Mater., 2019, 31, 1900592[11]
Gd_2O_3-Co/NG	-	114.3	600 s / cycle for 160 cycles	735 mAh g^{-1} at 5 mA cm^{-2}	Adv. Energy Mater., 2020, 10, 1903833[12]

References:

1. G. Kresse and J. Furthmuller, *Physical Review B*, 1996, **54**, 11169-11186.
2. J. P. Perdew, K. Burke and M. Ernzerhof, *Physical Review Letters*, 1996, **77**, 3865-3868.
3. J. A. Santana, J. Kim, P. R. C. Kent and F. A. Reboredo, *J. Chem. Phys.*, 2014, **141**.
4. X. X. Wang, J. Sunarso, Q. Lu, Z. L. Zhou, J. Dai, D. Q. Guan, W. Zhou and Z. P. Shao, *Advanced Energy Materials*, 2020, **10**.
5. W. Cheng, P. Yuan, Z. Lv, Y. Guo, Y. Qiao, X. Xue, X. Liu, W. Bai, K. Wang, Q. Xu and J. Zhang, *Applied Catalysis B: Environmental*, 2020, **260**, 118198.
6. D. Chen, J. Zhu, X. Mu, R. Cheng, W. Li, S. Liu, Z. Pu, C. Lin and S. Mu, *Applied Catalysis B: Environmental*, 2020, **268**, 118729.
7. N. K. Wagh, S. S. Shinde, C. H. Lee, J.-Y. Jung, D.-H. Kim, S.-H. Kim, C. Lin, S. U. Lee and J.-H. Lee, *Applied Catalysis B: Environmental*, 2020, **268**, 118746.
8. Y.-Q. Zhang, H.-B. Tao, Z. Chen, M. Li, Y.-F. Sun, B. Hua and J.-L. Luo, *Journal of Materials Chemistry A*, 2019, **7**, 26607-26617.
9. X. P. Han, X. F. Ling, Y. Wang, T. Y. Ma, C. Zhong, W. B. Hu and Y. D. Deng, *Angewandte Chemie-International Edition*, 2019, **58**, 5359-5364.
10. S. S. Shinde, C. H. Lee, J.-Y. Jung, N. K. Wagh, S.-H. Kim, D.-H. Kim, C. Lin, S. U. Lee and J.-H. Lee, *Energy & Environmental Science*, 2019, **12**, 727-738.
11. B.-Q. Li, C.-X. Zhao, S. Chen, J.-N. Liu, X. Chen, L. Song and Q. Zhang, *Adv. Mater.*, 2019, **31**, 1900592.
12. M. Li, Y. Wang, Y. Zheng, G. Fu, D. Sun, Y. Li, Y. Tang and T. Ma, *Advanced Energy Materials*, 2020, **10**, 1903833.